RSC Advances

PAPER

View Article Online
View Journal | View Issue

Cite this: *RSC Adv.*, 2025, **15**, 33695

A sustainable approach to the development and characterization of chitosan thiomer beads for the efficient removal of Cd(II) ions from aqueous effluents

Wesam Abd El-Fattah,[a] Ahlem Guesmi,[a] Naoufel Ben Hamadi,[a] Rana Yahya,[b] Thamer S. Alraddadi,[c] Ahmed Shahat[d] and Reda F. M. Elshaarawy *[d]

This study presents a facile protocol for fabricating a new sustainable biosorbent, cross-linked thiourea-chitosan thiomer beads (CLCTB), as an eco-friendly scavenger for Cd^{2+} ions from aqueous effluents. The success of the fabrication protocol was validated, and the molecular and morphological characteristics of the new scavenger were investigated using spectral, thermal, and microscopic analyses. SEM analysis revealed the highly porous nature of the new scavenger, which is favorable for metal ion adsorption. Batch adsorption experiments revealed optimal Cd^{2+} removal at pH 6, 45 min contact time, 0.5 g adsorbent dose, and ambient temperature (25–30 °C). Kinetic studies showed that the pseudo-second-order model best described the adsorption process, indicating that chemisorption was the dominant mechanism. With a maximum adsorption capacity of 199.69 mg g^{-1}, the Langmuir isotherm provided an optimal fit to the experimental data, proving CLCTB's high adsorption efficiency for Cd. The process was confirmed to be both spontaneous and exothermic through thermodynamic analysis. Additionally, the beads exhibited excellent reusability over six adsorption–desorption cycles, maintaining high performance, which highlights their potential for practical application in water treatment. This study presents CLCTB as a promising, sustainable, and eco-friendly adsorbent for the efficient removal of Cd from contaminated water.

Received 8th June 2025
Accepted 30th August 2025

DOI: 10.1039/d5ra04050g

rsc.li/rsc-advances

1. Introduction

Owing to its unique characteristics, chitosan has garnered significant attention in environmental applications, particularly for removal of heavy metal ions.[1] However, chitosan's applications are limited by its poor mechanical strength and swelling in aqueous solutions. Among the promising strategies to address these challenges, the crosslinking approach is at the forefront. For example, amino groups of chitosan react with glutaraldehyde, forming Schiff bases and a 3D network that improves adsorption and stability.[2] This crosslinking process not only improves the structural integrity of chitosan beads but also introduces additional binding sites for metal ions, making glutaraldehyde-crosslinked chitosan a superior adsorbent compared to native chitosan.[3] Moreover, this crosslinking reaction forms imine bridges between the polymer chains, creating a three-dimensional network structure.[4]

While crosslinking improves the mechanical properties of chitosan, further functionalization is often required to enhance its selectivity and capacity for specific metal ions, such as cadmium.[5] Recently, thiolated chitosan derivatives have emerged as promising biosorbents for removing heavy metal ions from aqueous solutions, due to their enhanced adsorption capabilities and environmentally friendly characteristics.[6,7] The incorporation of thiol groups (–SH) into chitosan improves its water solubility and ability to chelate heavy metal ions through stable complexes. Thiolated chitosan derivatives as biosorbents offer high adsorption capacity, selectivity towards specific metal ions, and potential for regeneration and reuse.[8] Thiol and chitosan's functional groups create synergistic effects, yielding a material with multiple adsorption mechanisms: ion exchange, chelation, and electrostatic interactions. This multi-functionality enables the material to capture metal ions from aqueous solutions, even at low concentrations.[9] The presence of thiol groups enhances adsorbent selectivity towards specific metal ions, a critical factor in complex wastewater matrices with multiple competing ions.[10]

[a]*Department of Chemistry, College of Science, Imam Mohammad Ibn Saud Islamic University (IMSIU), P.O. Box 5701, Riyadh 11432, Saudi Arabia*

[b]*Department of Chemistry, College of Science, University of Jeddah, Jeddah, Saudi Arabia*

[c]*Department of Chemistry, Faculty of Science, Islamic University of Madinah, Al-Madinah Al-Munawwarah 42351, Saudi Arabia*

[d]*Department of Chemistry, Faculty of Science, Suez University, 43533 Suez, Egypt. E-mail: reda.elshaarawy@suezuniv.edu.eg*

Heavy metal contamination of water, notably cadmium (Cd), is a global problem due to its toxicity and bioaccumulation, threatening ecosystems and human health.[10,11] The persistence, bioaccumulation potential, and toxicity (even at low concentrations) of this contaminant necessitate effective water removal.[12] Conventional techniques for cadmium removal from wastewater include chemical precipitation, ion exchange, membrane filtration, adsorption using natural and synthetic materials, and electrochemical treatment. However, these methods are often plagued by drawbacks, such as high operational costs, generation of secondary pollutants, and limited selectivity.[13]

Recent research has focused on developing advanced adsorbents and hybrid technologies to improve cadmium removal efficiency. To name a few, magnetic chitosan nanoparticles (NPs) were synthesized and employed to achieve the removal of 97.76 mg g^{-1} of Cd^{2+} ions.[14] A study used chitosan to modify fig branch biochar (FBB) to create chitosan-modified fig branch biochar (CMFBB) for removing Cd^{2+} from wastewater. A Cd^{2+} adsorption capacity of 62.25 mg g^{-1} was reported by the CMFBB.[15] Sahebjamee *et al.* used polyethyleneimine (PEI) to modify the chitosan/polyvinyl alcohol membrane to improve metal ion uptake.[16] At 25 °C and pH 6, the modified membrane showed an adsorption capacity of 112.13 mg g^{-1} for Cd^{2+} ions. Jasim *et al.* created a novel scavenger (CEP) by modifying chitosan with epichlorohydrin and a bidentate Schiff base ligand. For Cd(II) ions, this scavenger may have a maximum adsorption capability of 79 mg g^{-1}.[17]

Targeting the development of a sustainable eco-friendly biosorbent with superior adsorptive removal capacity, this study aims to synthesize glutaraldehyde crosslinked chitosan thiomer beads (CLCTB) and to comprehensively evaluate their structural, morphological, and adsorption properties for cadmium removal.

2. Material and methods

The specifications of the reagents, chemicals, and instruments, as well as the methodologies for analytical measurements, are detailed in the SI.

2.1. Synthesis

The stepwise protocol (CLCTB) was depicted in Scheme 1.

2.1.1. Synthesis of thiourea functionalized crosslinked chitosan beads (CLCTB). Using a slightly modified version of the earlier method reported by Elshaarawy *et al.*,[18] GCC beads were converted into their thiomer derivatives. In brief, 1.0 g of GCC was mixed with 50 mL of DIW while stirring. Concoruntly, 1.1 g of thiourea (3 mol equivalents) was gradually dissolved in a solution combining 1.5 mL DIW and 0.7 mL HCl (3 mol equivalents) in a separate beaker. After that, the thiourea solution slowly added to the GCC dispersion while swirling

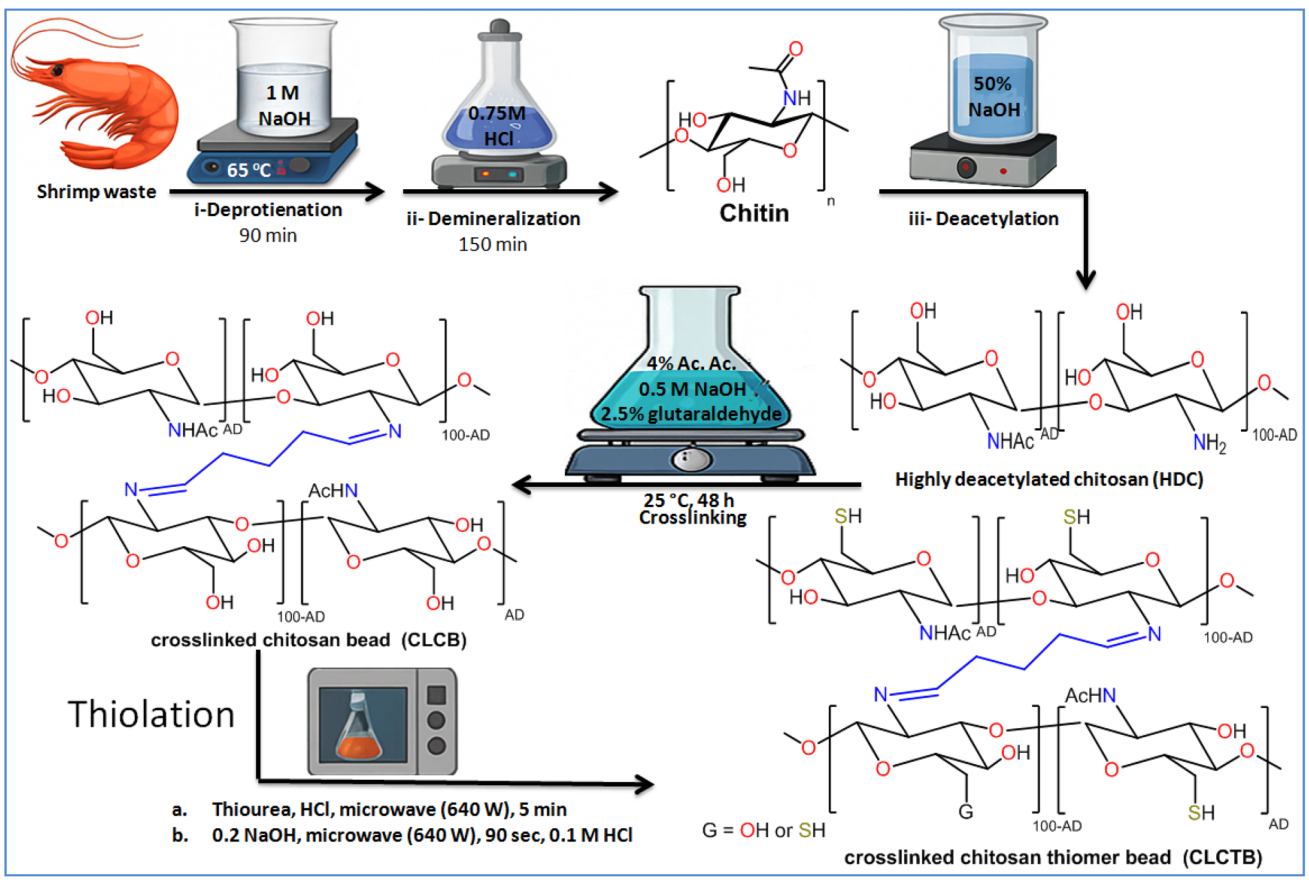

Scheme 1 A step-by-step protocol followed for the synthesis on new biosorbent (CLCTB).

vigorously for 10 min. The resultant combination was exposed to intermittent radiation at 10 s intervals for five min at 640 W of power. The generated intermediate was then hydrolyzed for 90 s at 640 W in a 0.2 N NaOH solution. After being taken out of the microwave, the solution was allowed to cool to room temperature. Ethanol was added after the cooled solution had been neutralized with 0.1 M HCl. After filtering and three acetone washes, the resulting white solid was dried at 50 °C.

2.2. Adsorption studies of Cd^{2+} ions on the CLCTB adsorbent

Before the adsorption tests, standard solutions of Cd^{2+} ions were prepared at a concentration of 1000 mg L^{-1}. The original solution stocks were diluted for the tests to reach the needed Cd^{2+} ion concentrations. Using 250 mL conical flasks, we performed all batch experiments with 100 mL of Cd^{2+} aqueous solutions and adsorbent samples. Atomic absorption spectroscopy was used to measure the Cd^{2+} ion concentration. We added a fixed mass of the prepared adsorbent to several Erlenmeyer flasks and then added 100 mL of a specified concentration to each flask. Using 0.1 M HCl/NaOH, the mixture's pH was adjusted to neutral. Investigations were conducted on the effects of operating variables in the pH range of 2–9, using an adsorbent dosage of 0.05. After equilibrium, the amount of adsorbed adsorbate on a clear metal sample was measured using atomic absorption spectrophotometry. Eqn (1), shown below, was used to assess the elimination mechanism's efficiency.

$$\%R = \frac{(C_0 - C_t)}{C_0} \times 100\sqrt{b^2 - 4ac} \quad (1)$$

where the final metal ion concentration in the desorption medium is C_t, and the initial concentration is C_0.

3. Results and discussion

3.1. Characterization

3.1.1. XRD. X-ray diffraction (XRD) analysis was conducted to investigate the crystalline construction of chitosan and CLCTB before and after Cd adsorption. The XRD patterns are presented in Fig. 1A. The XRD pattern of chitosan (Fig. 1A) shows a broad peak around $2\theta = 20.2°$ and 10.2°, which is characteristic of the semi-crystalline character of chitosan.[19] These peaks correspond to (101) and (002) planes of chitosan, indicating its partially ordered structure.[19]

Upon crosslinking chitosan with glutaraldehyde and thiolation with thiourea to form CLCTB, the intensity of this peak (20.2°) diminishes with slight negative shift, and new minor peaks suggest reduced crystallinity due to intermolecular crosslinks.[20] The crosslinking and functionalization processes have introduced amorphous regions into the polymer matrix.[21] The thiolation of GCC introduces structural modifications, resulting in new peaks at 2θ 25°, attributed to thiol groups' interaction with the chitosan matrix.[22]

After Cd^{2+} adsorption, the XRD pattern of CLCTB shows peak reduction, broadening, and slight shifts, with additional weak diffraction signals. The peak at $2\theta = 20°$ shows reduced intensity, indicating decreased crystallinity. This implies that Cd^{2+} ions disrupt the remaining ordered regions within the CLCTB matrix. Moreover, the appearance of new low-intensity peaks and shoulders within the 2θ range of 30–50°, which can be attributed to the formation of cadmium complexes,[23] suggests interactions between Cd^{2+} ions and the functional groups present in the polymer matrix. These interactions likely occur through chelation or complex formation.[23,24]

3.1.2. The thermal gravimetric analysis (TGA). The thermogravimetric analysis (TGA) curve of CLCTB reveals its thermal stability and decomposition behavior. As shown in Fig. 1B, CLCTB exhibits gradual weight loss starting at ~150 °C, with significant mass loss between 200 °C and 400 °C, followed by stabilization at elevated temperatures. Below 150 °C, weight loss of 10–15% results from the removal of physically adsorbed water and volatile compounds in the polymer matrix.[25] This behavior matches previously reported chitosan-based materials, where chitosan's hydrophilic nature leads to significant moisture absorption.[26] The weight loss between 150 °C and 250 °C corresponds to the decomposition of labile functional groups from the modification process, such as the breakdown of thiomethyl moieties or glycosidic bonds.[18,27] This degradation is less pronounced in native chitosan, showing the impact of modification on thermal stability.[28] The major mass loss between 200 °C and 400 °C represents the thermal degradation of the polymer backbone and the cross-linking structure. The decomposition temperature (T_d) at 5% weight loss for CLCTB was 285 °C, indicating improved thermal stability compared to native chitosan (250–270 °C) due to cross-linking effect.[29,30]

3.1.3. FTIR spectrum. The FTIR spectra of chitosan (CS), highly deacetylated chitosan (HDC), glutaraldehyde crosslinked chitosan beads (CLCB), and crosslinked chitosan thiomer beads (CLCTB) show differences in their functional groups due to chemical modifications (Fig. 1C). The O–H and N–H stretching peaks associated with the hydroxyl and amino groups in CS are typically observed as a broad band centered at 3360 cm^{-1}. Amide I (C═O stretch) and amide II (N–H bend and C–N stretch) bands can be seen at 1651 cm^{-1} and 1579 cm^{-1}. When comparing HDC and nascent CS FTIR spectra, significant changes in acetyl group peaks indicate substantial reduction in acetylation degree in HDC. Absorption bands for amide I and amide II groups occur near 1648 cm^{-1} and 1565 cm^{-1}. A decrease in amide I intensity with increases in amide II peak in the HDC spectrum indicates acetyl group removal and increased deacetylation degree.[31] Moreover, the ratio of absorbance at 1648 cm^{-1} to 3350 cm^{-1} quantifies deacetylation degree, and its decrease in HDC *versus* nascent chitosan confirms enhanced deacetylation.[32]

Comparing the FTIR spectrum of GCC beads with nascent HDC showed successful cross-linking, evidenced by a new absorption band at 1634 cm^{-1}, corresponding to imine bonds (C═N) formed between chitosan's amino groups and glutaraldehyde's aldehyde groups.[33] A shift in the N–H/OH stretching vibration peak suggests amino and hydroxyl groups involvement in cross-linking through H-bonding with imine linkage.[34] These spectral changes confirm the structural modification of

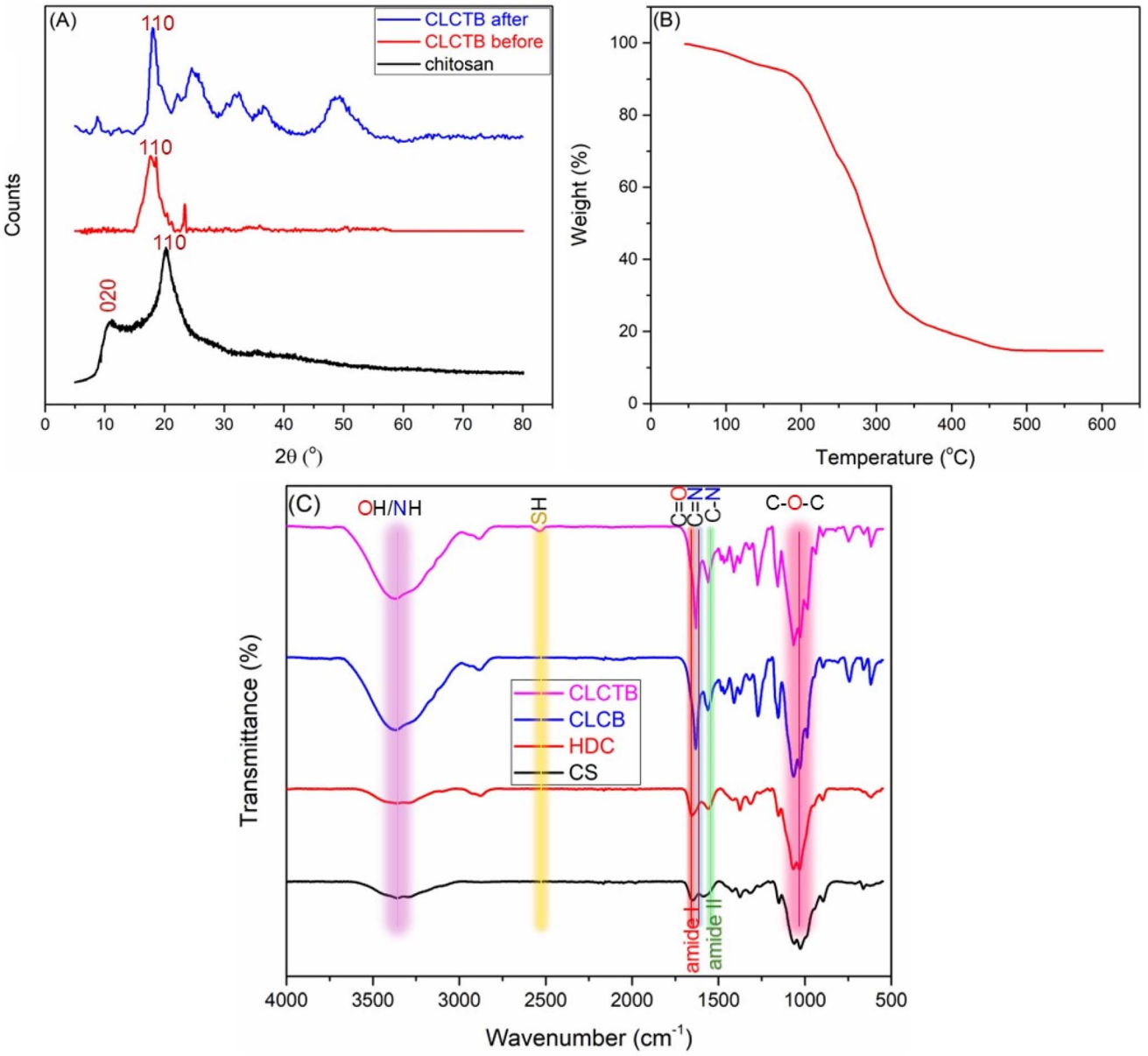

Fig. 1 (A) XRD diffraction patterns of chitosan, CLCTB before and after Cd adsorption. (B) TGA of curve of CLCTB. (C) FTIR spectra of CS, HDC, glutaraldehyde crosslinked chitosan beads (CLCB), and CLCTB.

chitosan and enhanced stability of the GCC network. The successful thiolation of GCC beads is confirmed by a weak broad band at 2530 in the CLCTB spectrum, characteristic of thiol (–SH) groups.[18] This new band appeared alongside GCC's characteristic peaks, indicating thiol functionalization was achieved while preserving the cross-linked chitosan structure.

3.1.4. Surface morphology (SEM). The SEM micrograph of CLCTB (Fig. 2A) shows a textured yet smooth surface with irregularities. The bead surface exhibits undulations and minor cracks from cross-linking and drying for SEM preparation.[35] These features align with previous observations of chitosan beads, where cross-linking affects surface topography.[36] Cross-sectional SEM micrographs show chitosan beads with interconnected pores ranging from 5 μm to 50 μm in diameter (Fig. 2B). The pore distribution and connectivity facilitate metal ion diffusion through the bead matrix, critical for cadmium adsorption efficiency.[37] The porous design creates large surface area for metal binding, with pore walls containing hydroxyl and amino groups that chelate Cd ions.[38]

After cadmium adsorption, SEM micrographs show changes in surface and internal structure (Fig. 2C). The surface appears rougher with cracks, due to metal ion binding.[39] The internal pores show reduced size and connectivity, indicating cadmium adsorption may cause partial collapse or blocking of pore entrances.[40] These morphological changes correlate with adsorption capacity, as structural modifications affect binding site accessibility within chitosan.[41]

3.1.5. Energy dispersive X-ray (EDX) analysis. Fig. 2D and E presents the EDX spectra of new biosorbent, CLCTB, before (A) and after (B) cadmium adsorption. CLCTB spectrum (Fig. 2D)

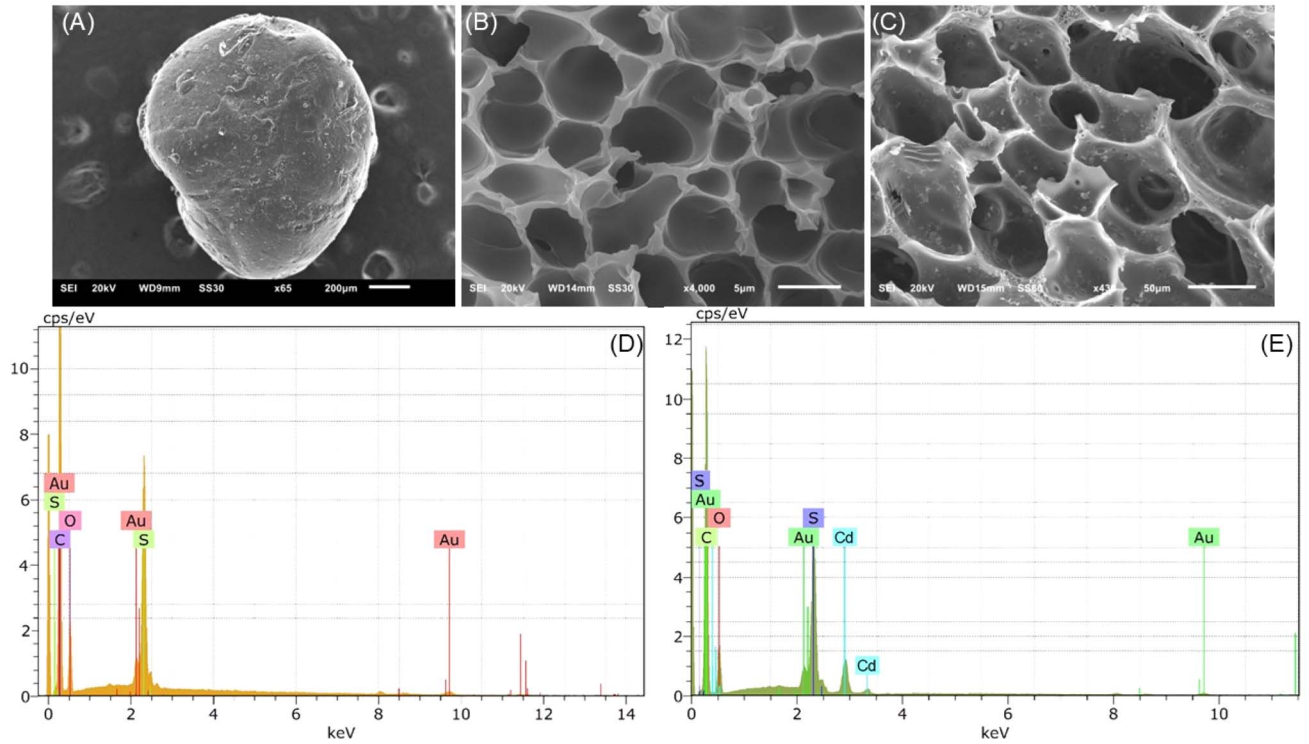

Fig. 2 SEM micrographs of: (A) the surface CLCTB (B) cross-section of CLCTB before Cd adsorption and (C) cross-section of CLCTB after Cd adsorption. (D and E) EDX spectra of the: (D) nascent CLCTB and (E) CLCTB after Cd adsorption.

exhibits prominent peaks for carbon (C, 0.27 keV), oxygen (O, 0.52 keV), sulfur (S, 2.3 keV), and a minor presence of gold (Au), due to coating for EDX measurement. Sulfur presence indicates successful chitosan thiolation through thiourea functionalization, enabling metal binding *via* sulfur atoms.

After exposure to Cd^{2+}, new peaks emerge at 3.1 and 3.3 keV in spectrum (Fig. 2E), confirming cadmium ion adsorption onto CLCTB bead surfaces. The consistent sulfur peak corroborates its role in cadmium binding. The unchanged elemental peaks for C, O, and S suggest the modified chitosan maintains structural integrity post-adsorption. Au peaks in both spectra are due to gold sputter-coating during SEM preparation and are unrelated to adsorption. The presence of cadmium peaks and key functional groups (S and N-containing) suggests adsorption occurred through group interactions rather than surface degradation or deposition. These findings align with the proposed ion exchange and electrostatic interactions discussed in previous sections, as well as the suggested adsorption mechanism involving chelation *via* thiol and amino functionalities.

3.2. Batch experiments

The adsorption effectiveness of cadmium ions (Cd^{2+}) on CLCTB was examined in batch adsorption studies by examining the effects of contact duration, pH, temperature, and adsorbent dosage. The experimental setup and results are discussed below.

3.2.1. Effect of pH. The pH significantly impacts the Cd adsorption capacity of our synthesized adsorbent. As shown in Fig. 3A, maximum adsorption occurs at pH 6 (optimal level), with efficiency rising from pH 2 to 6 before slightly decreasing. The adsorbent surface's functional groups' protonation/deprotonation explains this trend.[42] At lower pH values, the abundance of H^+ ions compete with Cd^{2+} ions for active sites on the chitosan derivative, reducing the adsorption efficiency.[7,10] Additionally, the thiol groups may remain protonated at lower pH, reducing their ability to coordinate with Cd^{2+}. The adsorption performance of the CLCTB is strongly influenced by the surface charge characteristics governed by the isoelectric point (IEP) of thiolated chitosan derivatives, which typically ranges between pH 2.6 and 5.9 for all reported thiolated chitosan derivatives.[7] Below the IEP, protonated imine and amino groups on the adsorbent create positive sites that hinder Cd^{2+} adsorption through electrostatic repulsion. Above the IEP, deprotonation creates negative sites on CLCTB, enhancing electrostatic attraction with Cd^{2+} ions. This behavior aligns with the optimal adsorption pH of 6 for CLCTB, where the surface is negatively charged, maximizing Cd^{2+} uptake *via* electrostatic interactions and chelation with thiol and amino groups.

3.2.2. Effect of contact time. Contact time plays a crucial role in determining adsorption process efficiency and capacity. At pH 6, cadmium ion adsorption efficiency by CLCTB was studied (Fig. 3B). Results show rapid adsorption reaching 70% within 20 min, with significant increase in the first 10 min. Beyond 30 min, adsorption efficiency approaches equilibrium, reaching 95% after 45 min. This follows typical kinetics, with rapid initial adsorption due to available active sites, followed by slowdown as the surface saturates.[43] The equilibrium time of

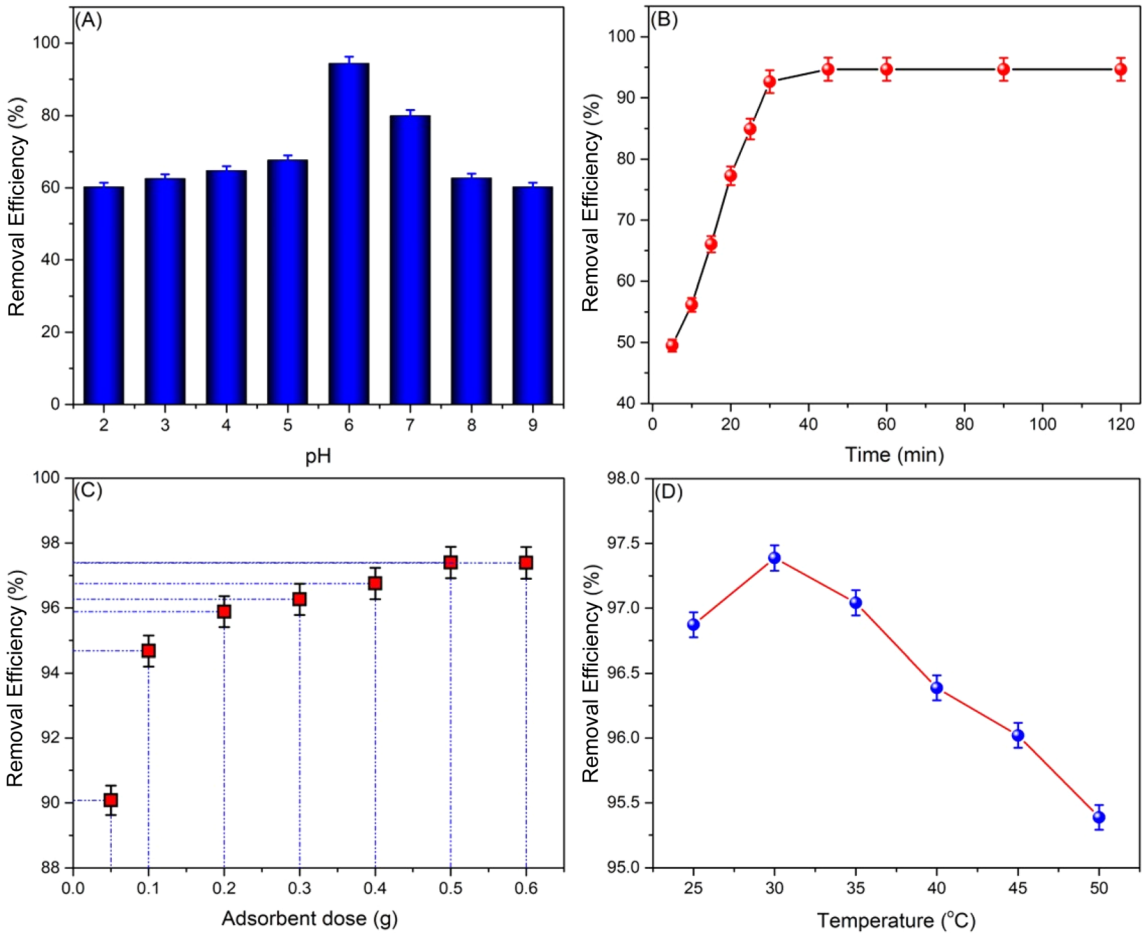

Fig. 3 (A) Effect of pH, (B) effect of contact time, (C) effect of adsorbent dose, (D) effect of temperature on the adsorption efficiency of CLCTB for Cd^{2+} ion removal.

45 min observed aligns with previous findings on chitosan-based adsorbents. Seyedi *et al.*[44] reported Cd adsorption on nanochitosan reaches equilibrium after 60 min, while Shekhawat *et al.*[23] found Cd^{2+} decontamination using thiourea-functionalized chitosan achieved equilibrium within 50 min. These findings confirm CLCTB is a promising adsorbent for cadmium elimination from contaminated water.

3.2.3. Effect of adsorbent dose. The biosorbent dose is crucial in determining the adsorption capacity and removal efficiency of Cd ions. The influence of biosorbent dosage (50 to 600 mg) on CLCTB adsorption was examined under optimal conditions (pH 6, duration 45 min) at ambient temperature (298 K). Adsorbent doses up to 0.5 g improved adsorption efficiency, while further dosage increases showed no significant benefits (Fig. 3C). This dose-dependent behavior relates to binding site availability; increasing biosorbent dose enhances surface area and active binding sites, improving Cd^{2+} uptake. However, beyond optimal dose, adsorption capacity may decrease due to site aggregation, reducing effective surface area for Cd^{2+} ions. Similar trends occur in crosslinked chitosan-based adsorbents, where increasing adsorbent dosage improves removal efficiency until equilibrium and site saturation.[45–47] A 97% removal rate was achieved with 0.5 g of CLCTB, representing peak removal efficiency.

3.2.4. Effect of medium temperature. Fig. 3D shows temperature's effect on CLCTB's adsorption efficiency for Cd^{2+} removal. The experiments were conducted from 25 °C to 50 °C. The efficiency increases slightly to a maximum at 30 °C (~97.5%), then decreases with higher temperatures. This trend suggests that the adsorption of Cd^{2+} ions onto CLCTB is exothermic. The initial enhancement in adsorption efficiency up to 30 °C occurs due to increased molecular motion, facilitating better interaction between Cd^{2+} ions and CLCTB binding sites. However, beyond 30 °C, adsorption efficiency decreases, likely due to weakened electrostatic interactions and desorption from increased thermal agitation. Elevated temperatures may disrupt coordinate bonds between cadmium and the sulfur/nitrogen atoms of thiomer groups. These findings align with previously reported studies on similar biosorbents,[48,49] where optimum adsorption occurs at moderate temperatures and declines with further heating.

Overall, the optimum parameters for Cd^{2+} ion removal by CLCTB are pH = 6, contact time = 45 min, adsorbent dose = 0.5 g, and temperature = 30 °C.

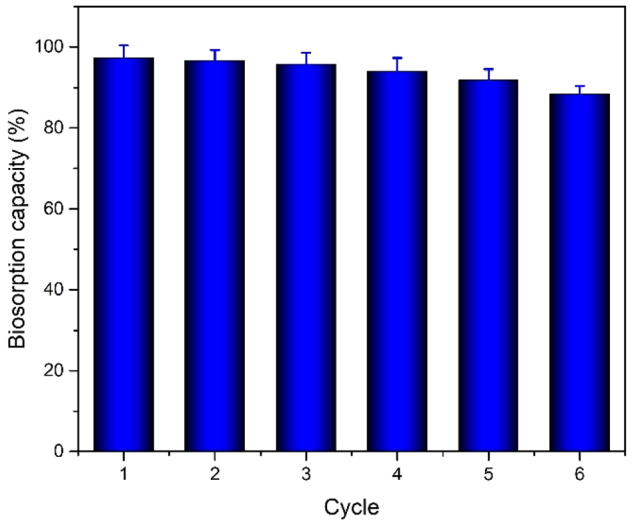

Fig. 4 CLCTB reusability for Cd^{2+} adsorption at optimal conditions (pH 6, 30 °C, 0.5 g adsorbent, 40 min).

3.2.5. The reusability test. Because it affects both environmental sustainability and commercial viability, adsorbent reusability is an essential metric for confirming practical potential. Reusing and regenerating an adsorbent lowers process expenses and lessens the environmental effects of producing and discarding new materials.[50] Therefore, the CLCTB reusability for Cd^{2+} adsorption was investigated under optimum conditions (Fig. 4). Impressively, the removal efficiency of CLCTB remains around 90% even after six cycles, with only a gradual and relatively minor decline in biosorption efficiency. With a mere 7.9% reduction in adsorption capacity after six cycles, CLCTB exhibits remarkable chemical resilience and substantial reuse potential, making it a viable option for real-world applications. The stability highlights the strength of the CLCTB architecture, which is improved by glutaraldehyde crosslinking.[51] This crosslinking enhances the mechanical strength of the chitosan matrix and stabilizes the thiol groups that coordinate with Cd^{2+}, thus reducing their leaching during desorption and regeneration processes.

3.3. Adsorption kinetics

Adsorption kinetics examine how adsorbate molecules move from solution to the adsorbent's surface, which is key for optimizing adsorption processes. The experimental data for Cd adsorption onto CLCTB were analyzed using pseudo-first-order, pseudo-second-order, Elovich, and intraparticle diffusion models to study the adsorption mechanism (refer to SI). Fig. 4 and Table 1 present the outcomes using various kinetic models and the corresponding fitting parameters for each model.

The pseudo-first-order model (Fig. 5A) yielded a relatively high correlation coefficient ($R^2 = 0.9641$), but the calculated equilibrium adsorption capacity ($q_e = 112.13$ mg g^{-1}) was significantly lower than the experimentally observed value ($q_e =$ 131.28 mg g^{-1}). This deviation suggests that the pseudo-first-order model does not adequately capture the adsorption process,[52] likely due to its assumption of simple physisorption on a homogeneous surface,[53] which does not reflect the complexity of the CLCTB adsorption mechanism.

The pseudo-second-order model (Fig. 5B) showed superior fit to experimental data with a high correlation coefficient ($R^2 =$ 0.9778). The calculated q_e (131.28 mg g^{-1}) matched the experimental value, confirming the model's accuracy. This fit indicates adsorption involves chemical interactions through electron sharing between cadmium ions and functional groups on the chitosan thiomer bead surface. The thiol and amino groups from thiourea modification enable coordination complexes with Cd^{2+}, resulting in chemically driven adsorption.[8,54]

Table 1 Fitting parameters for nonlinear kinetic and isotherm models

Kinetic model	Reduced chi^2	R^2	Parameter	Value	SD
Pseudo-1st order	47.95766	0.96412	q_e (mg g^{-1})	47.95766	4.5237
			$k_1 \times 10^{-3}$ (min^{-1})	9.766	0.01329
Pseudo-2nd order	29.74538	0.97775	q_e (mg g^{-1})	131.2849	6.1675
			$k_2 \times 10^{-4}$ (g mg^{-1} min)	9.418	2.042
Elovich	30.39748	0.97726	α	37.4271	11.8561
			β	0.03701	0.00444
Intraparticle diffusion	151.64128	0.88655	K_{diff} (mg g^{-1} $min^{-0.5}$)	14.8282	1.8606
			C	17.6659	8.9873
Isotherm model	**Reduced chi^2**	**R^2**	**Parameter**	**Value**	**SD**
Langmuir	19.75661	0.98538	q_{max} (mg g^{-1})	199.690	23.598
			$K_L \times 10^{-3}$ (L mg^{-1})	8.334	1.699
Freundlich	39.33833	0.97089	K_F (mg g^{-1})	3.6319	0.8745
			n	1.4462	0.1125
Temkin	150.60725	0.88856	α	0.2522	0.0543
			β	25.7325	2.8639
D–R	147.69351	0.89213	q_{max} (mg g^{-1})	108.579	11.912
			K_{D-R}	1579.73	505.31

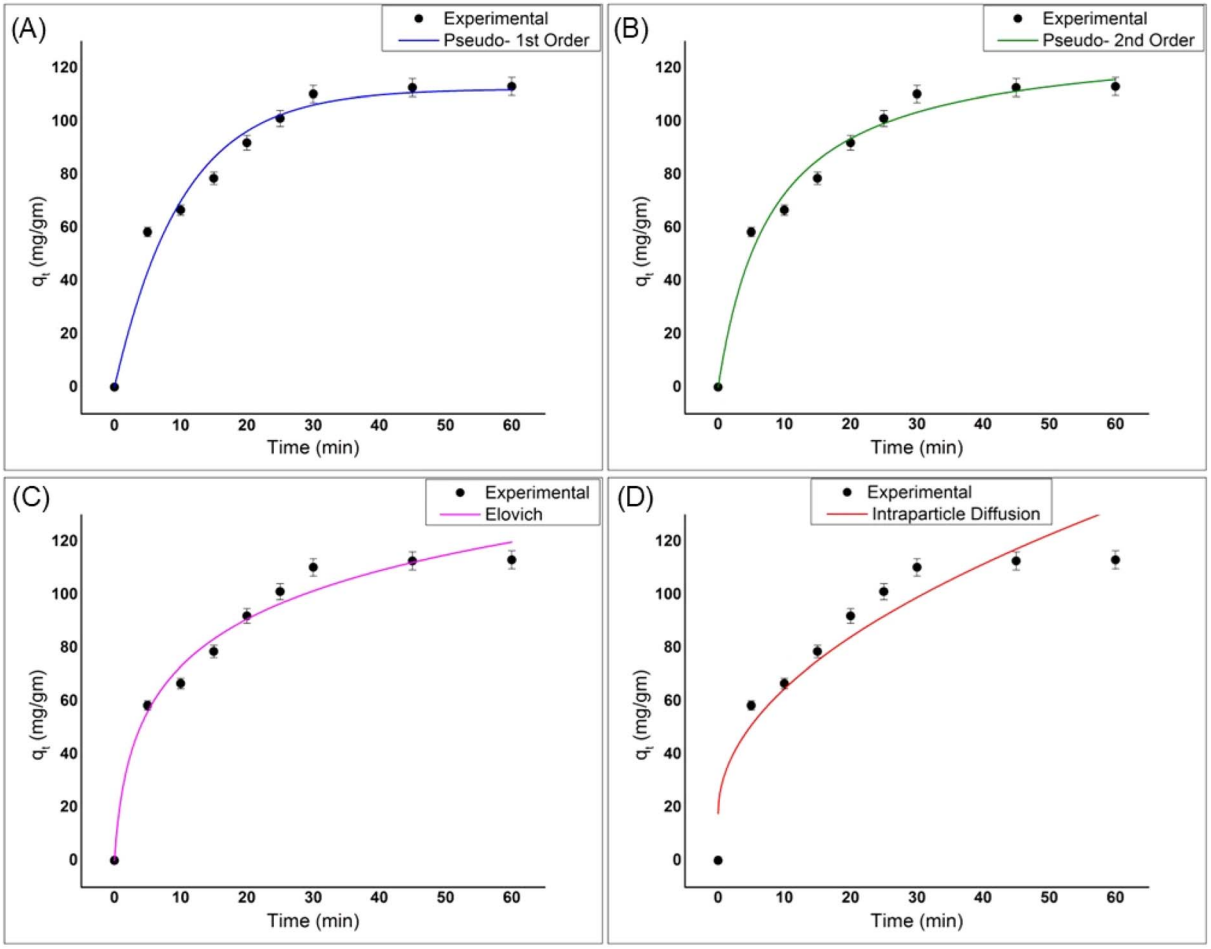

Fig. 5 The experimental data fitted to kinetic models (A) pseudo-first order (B) pseudo-second order (C) Elovich, and (D) intraparticle diffusion models.

The Elovich model (Fig. 5C), appropriate for heterogeneous surfaces with chemisorption, showed high correlation (R^2 = 0.9773), describing rapid initial adsorption and indicating varied activation energies on heterogeneous surfaces. The high adsorption rate (α = 37.43 mg g^{-1}) and desorption energy (β = 0.037 mg g^{-1}) reflect binding affinities from thiourea functionalization, enhancing adsorption under varying conditions.[55] Thus, the surface of CLCTB exhibits diverse active sites with varying activation energies, reflecting functional heterogeneity from thiourea grafting.

The intraparticle diffusion model showed moderate fit (R^2 = 0.8866) (Fig. 6D), indicating that intraparticle diffusion is involved but not the sole rate-limiting step.[56] The intercept (C = 17.67 mg g^{-1}) indicates external mass transfer controls initial rapid adsorption, while intraparticle diffusion governs the slower phase as Cd^{2+} ions penetrate pores. The kinetic data suggests Cd adsorption onto CLCTB occurs *via* chemisorption, with pseudo-second order and Elovich models fitting best. Initial uptake occurs through surface functional groups, while later stages involve cadmium diffusion into the bead's porous network. Glutaraldehyde cross-linking provides structural integrity, enabling high adsorption performance and reusability over multiple cycles.

3.4. Adsorption isotherm models

Adsorption isotherm models describe the relationship between adsorbate quantity and solution concentration, revealing equilibrium distribution mechanisms. These isotherms illuminate the adsorbent's adsorption capacity and surface properties. In this study, the experimental adsorption data were analyzed using four common isotherm models: Langmuir, Freundlich, Temkin, and Dubinin–Radushkevich (D–R),[57] with fitting results shown in Fig. 6 and parameters summarized in Table 1.

According to the obtained results, the Langmuir model provided an excellent fit to the data (R^2 = 0.985) (Fig. 6A), indicating predominant monolayer adsorption on a surface with uniform binding sites.[58] The maximum adsorption capacity (q_{max}) was calculated as 199.69 mg g^{-1}, reflecting the high affinity and adsorption capacity of CLCTB toward Cd^{2+} ions. The Langmuir constant ($K_L = 8.33 \times 10^{-3}$ L mg^{-1}) further confirms the strong interaction between the thiol functional groups and Cd^{2+} ions, consistent with the formation of coordination complexes. This chemical interaction enhances adsorption capacity, making CLCTB promising for heavy metal ion removal. The model assumes homogeneous surfaces

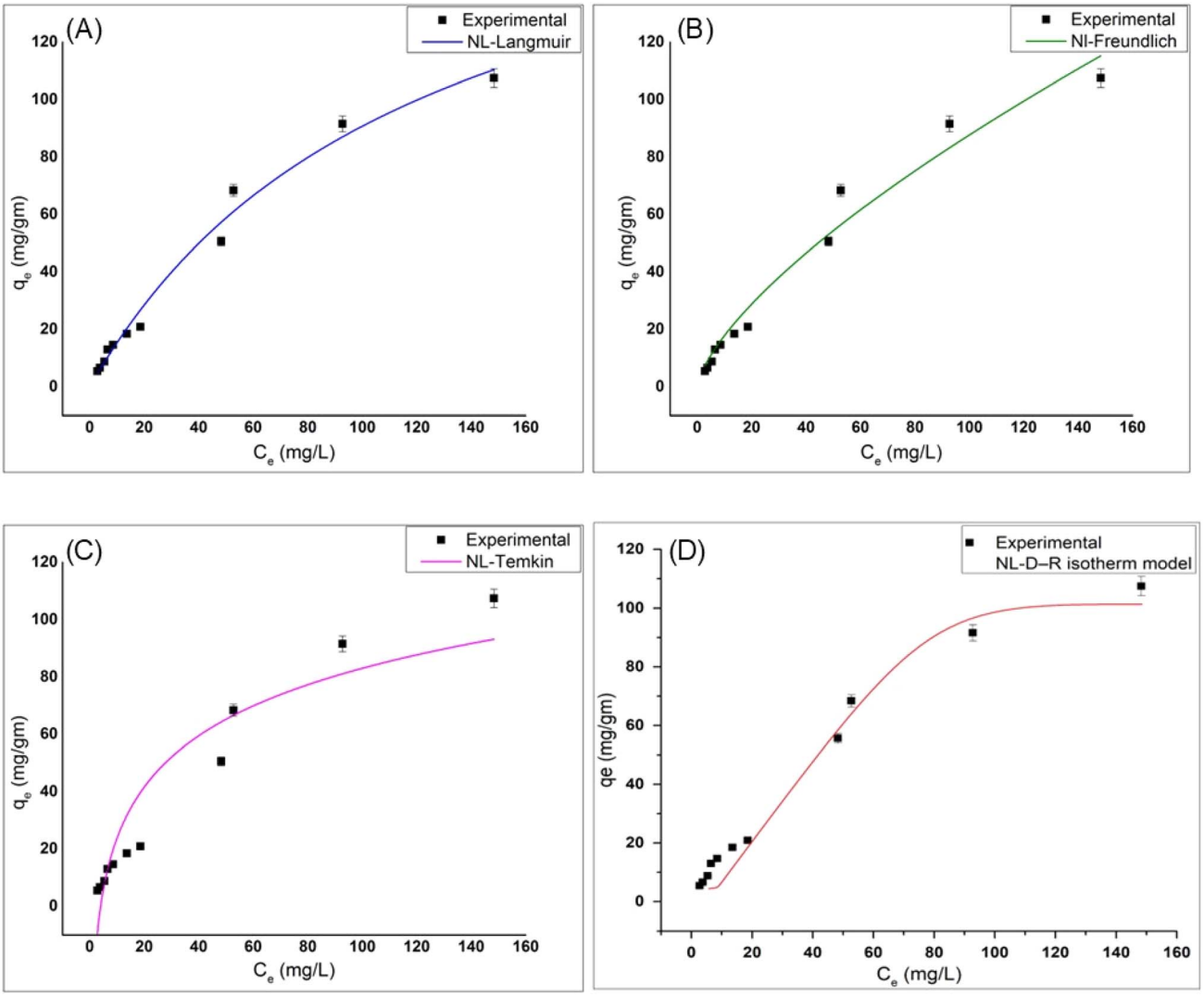

Fig. 6 The fitted experimental data for isotherm models (A) Langmuir (B) Freundlich (C) Temkin, and (D) D–R models.

without ion interaction, providing a framework for evaluating capacity and affinity.

The Freundlich model also fitted the data well (adjusted $R^2 = 0.971$) (Fig. 6B), suggesting that the adsorption process also involves heterogeneous surface energies and multilayer adsorption on the porous CLCTB beads.[58] The Freundlich constants, $K_F = 3.63$ mg g^{-1} and $n = 1.45$ (>1), indicate favorable adsorption conditions and a diverse range of binding affinities across the adsorbent surface, characteristic of heterogeneous adsorbents. This aligns with CLCTB nanoparticles' porous structure, allowing Cd^{2+} ions to adsorb on exterior surfaces and internal pores. As reported by Chen *et al.*,[59] the Freundlich model describes the adsorption behavior of metal ions onto porous adsorbents.

The Temkin model achieved a moderate fit ($R^2 = 0.88856$) (Fig. 6C), suggesting that adsorbate–adsorbate interactions influence the adsorption energy, which decreases linearly as surface coverage increases.[60] The Temkin parameters ($\alpha = 0.252$ and $\beta = 25.73$) indicate moderate adsorption heat, showing chemisorption influenced by cadmium ion interactions and surface heterogeneity. The Temkin model, while assuming uniform binding energy, provides insight into adsorption energetics on heterogeneous surfaces.

The D–R isotherm, which distinguishes between physical and chemical adsorption mechanisms,[61] fit the data moderately well ($R^2 = 0.89213$) (Fig. 6D). The maximum adsorption capacity from D–R was 108.58 mg g^{-1}, while the mean adsorption free energy ($E \approx 16.1$ kJ mol^{-1}) falls within the range typical for chemisorption, confirming strong coordination between Cd^{2+} ions and thiourea groups on CLCTB. This aligns with reports showing thiol-functionalized adsorbents form stable complexes with metal ions *via* coordination bonding.[62] The D–R model assumes constant adsorption potential and may not capture surface heterogeneity but confirms the chemical interaction nature.

The comprehensive analysis of isotherm models shows that Cd^{2+} adsorption onto CLCTB is characterized by monolayer chemisorption with strong affinity between adsorbent and

adsorbate, evidenced by high correlation with the Langmuir model ($R^2 = 0.98538$).[63] Meanwhile, the porous and heterogeneous structure of CLCTB facilitates multilayer adsorption and interactions among adsorbate molecules, supported by significant correlation with the Freundlich model ($R^2 = 0.97089$).[64] The coordination between thiourea groups and cadmium ions contributes to high adsorption capacity. These findings position CLCTB as an effective adsorbent for cadmium removal, combining substantial capacity with surface heterogeneity. The chemical stability and reusability of CLCTB make it practical for wastewater treatment, offering an environmentally friendly approach to heavy metal remediation.

3.5. Thermodynamic study

The thermodynamic parameters of Cd^{2+} adsorption onto CLCTB, including Gibbs free energy change (ΔG°), enthalpy change (ΔH°), and entropy change (ΔS°), were calculated at different temperatures ranging from 298.15 K to 333.15 K and are summarized in Fig. S1 and Table S1 (SI). The negative values of ΔG° at all tested temperatures (*e.g.*, −58.97 to −63.00 kJ mol^{-1}) clearly indicate that the adsorption of Cd^{2+} onto CLCTB is a spontaneous process. Moreover, the increasing magnitude of ΔG° with rising temperature suggests that higher temperatures favor adsorption, pointing to an endothermic mechanism. This trend is consistent with prior studies involving heavy metal adsorption onto chitosan-based or thiourea-functionalized materials.[54,65] The positive value of entropy change ($\Delta S^\circ = +115.27$ J mol^{-1} K^{-1}) reflects an increase in randomness at the solid–solution interface during Cd^{2+} uptake. This could be attributed to the displacement of water molecules coordinated to Cd^{2+}, as well as structural rearrangement within the CLCTB network that facilitates ion binding. A similar positive entropy shift has been reported for Cd^{2+} or Pb^{2+} adsorption onto crosslinked thiourea or amine-rich biopolymers.[66] The enthalpy change ($\Delta H^\circ = +24.60$ kJ mol^{-1}) being positive confirms the endothermic nature of the process, suggesting that energy input enhances adsorption performance, likely due to increased pore accessibility and enhanced ion mobility at higher temperatures. This value falls within the range reported for chemisorption-dominant mechanisms, where interactions such as complexation or coordination with functional groups like –NH_2, –SH, or –C═S are prevalent.[66,67] Taken together, the thermodynamic profile ($\Delta G^\circ < 0$, $\Delta H^\circ > 0$, $\Delta S^\circ > 0$) confirms that Cd^{2+} adsorption onto CLCTB is spontaneous, endothermic, and entropy-driven, likely involving strong interactions between Cd^{2+} and the thiourea functional groups embedded in the chitosan matrix.

3.6. Comparative analysis of CLCTB with reported chitosan-based adsorbents

Table 2 presents a comparative overview of the cadmium adsorption capacities of the glutaraldehyde cross-linked chitosan thiomer beads (CLCTB) alongside various chitosan-based adsorbents from literature. The adsorption capacity of CLCTB (199.69 mg g^{-1}) exceeds previously reported materials, which range from 34.68 mg g^{-1} to 126.65 mg g^{-1}. In addition, compared to other systems that require up to 120 min or longer, CLCTB's comparatively short equilibrium time (45 min) highlights its quick adsorption kinetics. This superior performance stems from the functionalization of chitosan with thiol groups and cross-linking by glutaraldehyde, which enhance the number and strength of active binding sites for cadmium ions. The thiol moieties introduce sulfur and nitrogen donor atoms capable of strong coordination with Cd^{2+}, while the cross-linked structure provides mechanical stability and maintains porosity, facilitating efficient ion adsorption. This combination results in enhanced chemisorption capacity and stability, outperforming other chitosan-based adsorbents that rely on different functional groups or composites. These findings demonstrate CLCTB as a high-performance adsorbent for cadmium removal in water treatment applications, offering improved capacity while maintaining structural integrity and reusability. The promising adsorption capacity of CLCTB indicates its potential for practical deployment in environmental remediation.

Table 2 Comparative analysis of CLCTB with reported chitosan-based adsorbents for Cd^{2+} removal

		Optimum conditions						
Nr	Sorbent	Dose	pH	Time	$[Cd]_{initial}$	Temp. (°C)	q_{max} (mg g^{-1})	Ref.
1	EDTA-crosslinking-chitosan/polypyrrole composites	0.33 g	6	24 h	30 mg L^{-1}	25	68.31	68
2	Chitosan-based nano-sorbents	1.0 g L^{-1}	6	30 min	50 mg L^{-1}	30	92.50	69
3	Magnetic chitosan-mediated GO	10 mg	6	60 min	100 mg L^{-1}	25	39.35	70
4	Chitosan@activated carbon composite	0.02 g	6	120 min	50 mg L^{-1}	30	84.75	71
5	Ni–Fe layered double hydroxide and chitosan composite	15 mg	6	30 min	50 mg L^{-1}	25	34.68	72
6	Chitosan/nano-hydroxyapatite composite	0.5 g	6	120 min	100 mg L^{-1}	25	126.65	73
7	Chitosan-modified MXene (CSMX)	0.5 g	6	90 min	50 mg L^{-1}	25	93.07	74
8	Amino-modified chitosan/gold tailings composite	0.4 g	6	120 min	100 mg L^{-1}	25	99.46	75
9	Magnetic chitosan-salicylaldehyde Schiff base	0.1 g	5.5	120 min	100 mg L^{-1}	25	114.80	76
10	CLCTB	0.5 g	6	45 min	10 mg L^{-1}	30	199.69	TW[a]

[a] TW = this work.

3.7. The proposed adsorption mechanism

Fig. 7 depicts the mechanism of how Cd^{2+} adsorbs onto CLCTB, with shifts in FTIR spectra (Fig. 7A) and a schematic representation (Fig. 7B) of the proposed mechanism. This illustration serves to underscore the importance of not only the structural design of the adsorbent material but also of its surface functional groups. Although the FTIR technique is not very surface-sensitive and gives an average picture of what is happening both on the surface and in the bulk, it can still show trends and detect changes that occur upon adsorption. Therefore, upon adsorption, the FTIR spectra show clear shifts of almost all the key vibrational bands of the functional groups that are most likely involved in the adsorption process. The thiol (–SH) stretching band at 2530 cm^{-1} has disappeared, as shown in Fig. 7A, suggesting the thiol group has deprotonated and sulfur has coordinated with cadmium. This implies an ion exchange process replaces the hydrogen atom of thiol groups with cadmium ions. Furthermore, cadmium ions are drawn to the negatively charged thiolate group by electrostatic attraction.[7] The wide stretching band of –OH and –NH around 3350 cm^{-1} narrows, indicating coordination with Cd^{2+}. The NH_2 bending vibrations (1575 cm^{-1}) and C=N (imine) band (1634 cm^{-1}) are shifted, suggesting Cd^{2+} ions coordinate with the amine and imine functionalities of the modified chitosan matrix.

The mechanism includes both chemisorption and physisorption, as shown in Fig. 7B. Schiff base cross-linking, which is facilitated by glutaraldehyde, adds imine functionalities as coordination sites and increases the structural rigidity of the bead. While amine and hydroxyl groups stabilize metal binding through electrostatic interactions and hydrogen bonding, thiol groups offer high-affinity soft donor sites for Cd^{2+} through thiolate coordination. Furthermore, CLCTB's crosslinked network-enabled porous structure makes it easier for Cd^{2+} to diffuse and reach internal binding sites, which helps explain the high adsorption capacity that has been noted. Because of the porous structure created by this cross-linked network, Cd^{2+} can efficiently access internal binding sites. CLCTB is a strong biosorbent for heavy metal remediation in cadmium-contaminated environments due to the synergy between its physical architecture and chemical functionality, which allows for a high adsorption capacity.[77]

Interestingly, the features of the CLCTB support sustainability in several keyways. First, the core biopolymer, chitosan, is derived from natural sources, biodegradable, and renewable. Second, the process that converts chitosan into thiolated chitosan, the basic functional form of the polymer, does not use any hazardous reagents and enhances the metal-chelating capacity of the biopolymer. This is, again, a green chemistry process. Third, crosslinking with glutaraldehyde stabilizes the bead structure and provides mechanical robustness for long-term stability. Additionally, the high capacity for adsorbing Cd(II) ions (199.69 mg g^{-1}) and the good performance over six

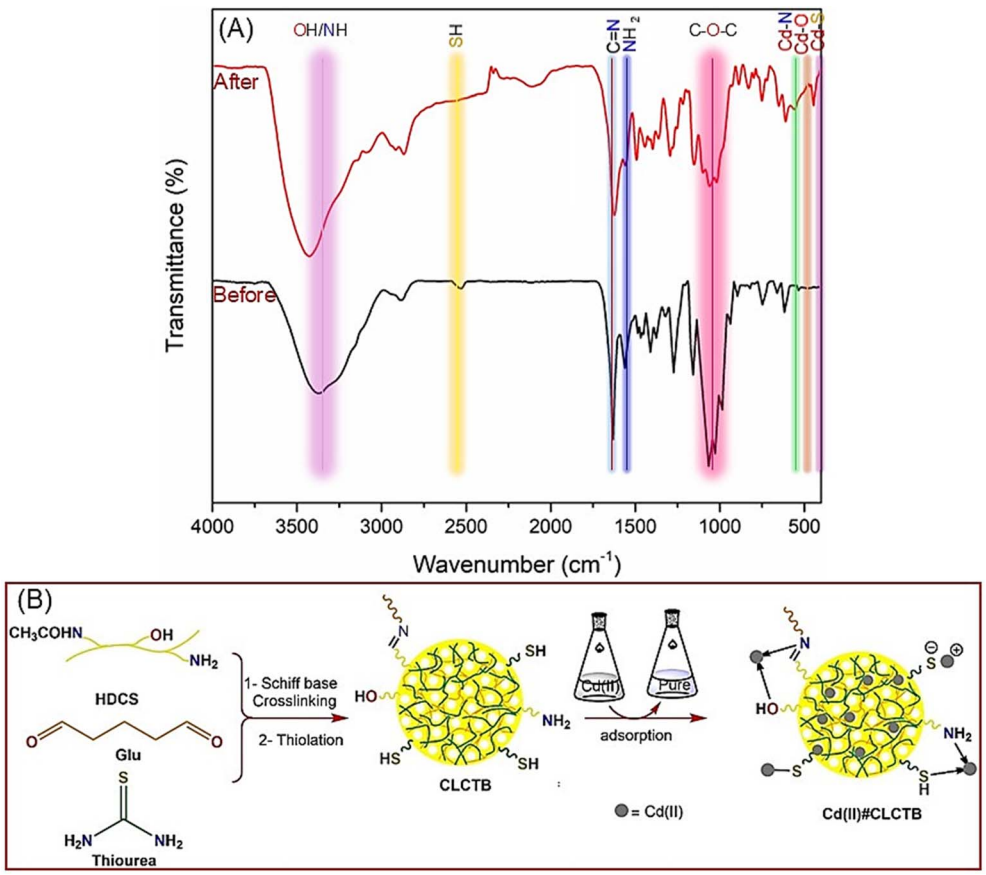

Fig. 7 (A) FTIR spectra of glutaraldehyde crosslinked chitosan thiol beads (CLCTB) before after Cd^{2+} adsorption. (B) The possible mechanism for adsorption of cadmium ions onto CLCTB.

adsorption–desorption cycles with minimal loss of efficiency (<10%) make it reusable. Finally, the fabrication process works under mild conditions and necessitates no toxic solvents, which minimizes environmental repercussions. These characteristics demonstrate that CLCTB is effective, environmentally responsible, and economically viable for wastewater treatment, making it a sustainable adsorbent.

4. Conclusion

This study successfully synthesized and characterized glutaraldehyde cross-linked thiourea functionalized chitosan beads (CLCTB) for efficient cadmium (Cd^{2+}) adsorption. Structural and morphological analyses using XRD, FTIR, SEM, TEM, and EDS confirmed the successful incorporation of thiourea groups and cross-linking, along with enhanced porosity and surface functionality. The modified beads exhibited improved thermal stability, with a decomposition temperature of 285 °C, and showed optimal Cd^{2+} removal at pH 6, 45 minutes contact time, 0.5 g adsorbent dose, and 25–30 °C. Kinetic studies revealed that the adsorption process obeyed a pseudo-second-order model, implying chemisorption as the primary mechanism. Isotherm data fit well with the Langmuir model, yielding a high maximum adsorption capacity of 199.69 mg g^{-1}. The CLCTB showed great reusability, maintaining over 95% efficiency through six adsorption–desorption cycles. The adsorption mechanism involved electrostatic interactions, coordinate covalent bonding, and ion exchange, with thiourea groups providing strong binding sites for cadmium ions. The cross-linking with glutaraldehyde enhanced structural stability, preventing swelling and degradation in aqueous environments. Overall, CLCTB proves to be a promising, sustainable, and eco-friendly adsorbent for cadmium removal from contaminated water. This work contributes to the development of effective solutions for heavy metal pollution and provides a foundation for future research on optimizing synthesis methods and expanding application to other metal ions.

Conflicts of interest

We confirm that there are no known conflicts of interest associated with this publication and there has been no significant financial support for this work that could have influenced its outcome.

Data availability

The data that support the findings of this study are available from the corresponding author upon reasonable request.

Supplementary information is available. See DOI: **https://doi.org/10.1039/d5ra04050g**.

Acknowledgements

This work was supported and funded by the Deanship of Scientific Research at Imam Mohammad Ibn Saud Islamic University (IMSIU) (grant number IMSIU-DDRSP2502).

References

1 R. Yahya and R. F. M. Elshaarawy, *Int. J. Biol. Macromol.*, 2024, **277**, 134350.
2 D. Y. Pratt, L. D. Wilson and J. A. Kozinski, *J. Colloid Interface Sci.*, 2013, **395**, 205–211.
3 T.-Y. Hsien and G. L. Rorrer, *Ind. Eng. Chem. Res.*, 1997, **36**, 3631–3638.
4 Q. Li, H. Su, Y. Yang, J. Zhang, C. Xia and Z. Guo, *Environ. Sci.: Water Res. Technol.*, 2023, **9**, 294–307.
5 B. Wang, Y. Zhu, Z. Bai, R. Luque and J. Xuan, *Chem. Eng. J.*, 2017, **325**, 350–359.
6 S. K. Yong, N. S. Bolan, E. Lombi, W. Skinner and E. Guibal, *Crit. Rev. Environ. Sci. Technol.*, 2013, **43**, 1741–1794.
7 F. Seidi, M. Reza Saeb, Y. Huang, A. Akbari and H. Xiao, *Chem. Rec.*, 2021, **21**, 1876–1896.
8 S. K. Yong, N. Bolan, E. Lombi and W. Skinner, *Water, Air, Soil Pollut.*, 2013, **224**, 1–12.
9 X. Song, L. Li, L. Zhou and P. Chen, *Chem. Eng. Res. Des.*, 2018, **136**, 581–592.
10 K. Chauhan, P. Singh and R. K. Singhal, *ACS Appl. Mater. Interfaces*, 2015, **7**, 26069–26078.
11 M. Wang, Z. Chen, W. Song, D. Hong, L. Huang and Y. Li, *Bull. Environ. Contam. Toxicol.*, 2021, **106**, 65–74.
12 R. Ankush, S. Lamba, D. Deepika and R. Prakash, *Cadmium Toxicity in Water: Challenges and Solutions*, 2024, pp. 3–20.
13 J. Ayach, W. El Malti, L. Duma, J. Lalevée, M. Al Ajami, H. Hamad and A. Hijazi, *Polymers*, 2024, **16**, 1959.
14 H. Zhang, X. Tan, T. Qiu, L. Zhou, R. Li and Z. Deng, *Int. J. Biol. Macromol.*, 2019, **141**, 1165–1174.
15 F. Xiao, D. Su, Y. Ren, J. Zhou, H. Xu, Z. Li and J. He, *Langmuir*, 2025, **41**(6), 3909–3921.
16 N. Sahebjamee, M. Soltanieh, S. M. Mousavi and A. Heydarinasab, *Carbohydr. Polym.*, 2019, **210**, 264–273.
17 S. A. Jasim, K. Hachem, S. Abed Hussein, A. Turki Jalil, N. M. Hameed and A. Dehno Khalaji, *J. Chin. Chem. Soc.*, 2022, **69**, 1051–1059.
18 R. F. M. Elshaarawy, L. A. Ismail, M. Y. Alfaifi, M. A. Rizk, E. E. Eltamany and C. Janiak, *Int. J. Biol. Macromol.*, 2020, **152**, 709–717.
19 Y. Zhang, C. Xue, Y. Xue, R. Gao and X. Zhang, *Carbohydr. Res.*, 2005, **340**, 1914–1917.
20 G. L. Clark and A. F. Smith, *J. Phys. Chem.*, 2002, **40**, 863–879.
21 J. M. Frick, A. Ambrosi, L. D. Pollo and I. C. Tessaro, *J. Polym. Environ.*, 2018, **26**, 2748–2757.
22 B. Han, Y. Wei, X. Jia, J. Xu and G. Li, *J. Appl. Polym. Sci.*, 2012, **125**, E143–E148.
23 A. Shekhawat, S. Kahu, D. Saravanan and R. Jugade, *Curr. Res. Green Sustainable Chem.*, 2022, **5**, 100246.
24 A. K. Mishra and A. K. Sharma, *Int. J. Biol. Macromol.*, 2011, **49**, 504–512.
25 J. Alkabli, M. A. Rizk, R. F. M. Elshaarawy and W. N. El-Sayed, *Int. J. Biol. Macromol.*, 2021, **184**, 454–462.
26 N. S. Lebedeva, S. S. Guseinov, E. S. Yurina, Y. A. Gubarev and O. I. Koifman, *Int. J. Biol. Macromol.*, 2019, **137**, 1153–1160.

27 R. Bhatt and P. P, *Carbohydr. Polym.*, 2019, **207**, 663–674.
28 P. Z. Hong, S. D. Li, C. Y. Ou, C. P. Li, L. Yang and C. H. Zhang, *J. Appl. Polym. Sci.*, 2007, **105**, 547–551.
29 M. Pieróg, J. Ostrowska-Czubenko and M. Gierszewska-Drużyńska, *Progress on Chemistry and Application of Chitin and its Derivatives*, 2012, pp. 71–78.
30 J. Zawadzki and H. Kaczmarek, *Carbohydr. Polym.*, 2010, **80**, 394–400.
31 K. V. H. Prashanth, F. S. Kittur and R. N. Tharanathan, *Carbohydr. Polym.*, 2002, **50**, 27–33.
32 S. Mima, M. Miya, R. Iwamoto and S. Yoshikawa, *J. Appl. Polym. Sci.*, 1983, **28**, 1909–1917.
33 E. Mirzaei B, A. Ramazani Sa, M. Shafiee and M. Danaei, *Int. J. Polym. Mater. Polym. Biomater.*, 2013, **62**, 605–611.
34 B. Li, C.-L. Shan, Q. Zhou, Y. Fang, Y.-L. Wang, F. Xu, L.-R. Han, M. Ibrahim, L.-B. Guo and G.-L. Xie, *Mar. Drugs*, 2013, **11**, 1534–1552.
35 S. R. Akaji and D. Dewez, *Int. J. Biomater.*, 2020, **2020**, 4158086.
36 M. H. Mahaninia and L. D. Wilson, *J. Appl. Polym. Sci.*, 2016, **133**, 42949.
37 S. Nisar, A. H. Pandit, L.-F. Wang and S. Rattan, *RSC Adv.*, 2020, **10**, 14694–14704.
38 L. Chen, P. Wu, M. Chen, X. Lai, Z. Ahmed, N. Zhu, Z. Dang, Y. Bi and T. Liu, *Appl. Clay Sci.*, 2018, **159**, 74–82.
39 S. S. Salih and T. K. Ghosh, *Cogent Environ. Sci.*, 2017, **3**, 1401577.
40 S. J. Wu, T. H. Liou, C. H. Yeh, F. L. Mi and T. K. Lin, *J. Appl. Polym. Sci.*, 2013, **127**, 4573–4580.
41 M. A. A. Aljar, S. Rashdan, A. Almutawah and A. A. El-Fattah, *Gels*, 2023, **9**, 328.
42 L. Zhang, Y. Zeng and Z. Cheng, *J. Mol. Liq.*, 2016, **214**, 175–191.
43 E. M. Saad, R. F. Elshaarawy, S. A. Mahmoud and K. M. El-Moselhy, *J. Bioresour. Bioprod.*, 2021, **6**, 223–242.
44 S. M. Seyedi, B. Anvaripour, M. Motavassel and N. Jadidi, *Int. J. Eng. Innov. Technol.*, 2013, **2**, 145–148.
45 D. Zhang, G. Crini, E. Lichtfouse, B. Rhimi and C. Wang, *Chem. Rec.*, 2020, **20**, 1220–1234.
46 P. Shankar, T. Gomathi, K. Vijayalakshmi and P. N. Sudha, *Int. J. Biol. Macromol.*, 2014, **67**, 180–188.
47 M. Kumar, B. P. Tripathi and V. K. Shahi, *J. Hazard. Mater.*, 2009, **172**, 1041–1048.
48 M. Li, Z. Zhang, R. Li, J. J. Wang and A. Ali, *Int. J. Biol. Macromol.*, 2016, **86**, 876–884.
49 F. Zhao, E. Repo, D. Yin and M. E. T. Sillanpää, *J. Colloid Interface Sci.*, 2013, **409**, 174–182.
50 A. H. Khan, N. A. Khan, M. Zubair, M. A. Shaida, M. S. Manzar, A. Abutaleb, M. Naushad and J. Iqbal, *Environ. Res.*, 2022, **204**, 112243.
51 W. S. W. Ngah, C. S. Endud and R. Mayanar, *React. Funct. Polym.*, 2002, **50**, 181–190.
52 Z. A. Sutirman, M. M. Sanagi, K. J. Abd Karim, W. A. W. Ibrahim and B. H. Jume, *Int. J. Biol. Macromol.*, 2018, **116**, 255–263.
53 J. Wang and X. Guo, *Crit. Rev. Environ. Sci. Technol.*, 2023, **53**, 1837–1865.
54 N. A. Alamrani, F. M. Almutairi, F. A. Alotaibi, D. A. K. Alenazi, M. Monier, D. A. Abdel-Latif and N. H. Elsayed, *Mater. Today Chem.*, 2023, **30**, 101547.
55 A. A. Abia, O. B. Didi and E. D. Asuquo, *J. Appl. Sci.*, 2006, **6**, 2549–2556.
56 J. R. Evans, W. G. Davids, J. D. MacRae and A. Amirbahman, *Water Res.*, 2002, **36**, 3219–3226.
57 M. A. Al-Ghouti and D. A. Da'ana, *J. Hazard. Mater.*, 2020, **393**, 122383.
58 A. K. Mallik, S. M. F. Kabir, F. B. A. Rahman, M. N. Sakib, S. S. Efty and M. M. Rahman, *J. Environ. Chem. Eng.*, 2022, **10**, 108048.
59 X. Chen, M. F. Hossain, C. Duan, J. Lu, Y. F. Tsang, M. S. Islam and Y. Zhou, *Chemosphere*, 2022, **307**, 135545.
60 K. H. Chu, *Ind. Eng. Chem. Res.*, 2021, **60**, 13140–13147.
61 B. Mahanty, S. K. Behera and N. K. Sahoo, *Sep. Sci. Technol.*, 2023, **58**, 1275–1282.
62 V. P. Kothavale, A. Sharma, R. P. Dhavale, V. D. Chavan, S. R. Shingte, O. Selyshchev, T. D. Dongale, H. H. Park, D. R. T. Zahn and G. Salvan, *J. Phys. Chem. Solids*, 2023, **172**, 111089.
63 F. Xiao, D. Su, Y. Ren, J. Zhou, H. Xu, Z. Li and J. He, *Langmuir*, 2025, **41**, 3909–3921.
64 E. Radha, T. Gomathi, P. N. Sudha, S. Latha, A. A. Ghfar and N. Hossain, *Biomass Convers. Biorefin.*, 2025, **15**, 1847–1862.
65 C.-A. Ghiorghita, M. M. Lazar, I.-V. Platon, D. Humelnicu, F. Doroftei and M. V. Dinu, *Int. J. Biol. Macromol.*, 2023, **235**, 123910.
66 Z. Yang, X. Huang, X. Yao and H. Ji, *J. Appl. Polym. Sci.*, 2018, **135**, 45568.
67 J. S. Alnawmasi, *Carbohydr. Polym.*, 2023, **308**, 120596.
68 Y. Shi, J. Feng, Z. Zhang, N. Cao, J. Li, H. Li, L. Li, Q. Hua, Q. Ma and K. Zhang, *Sep. Purif. Technol.*, 2023, **327**, 124926.
69 D. Chandra, M. T. H. Molla, M. A. Bashar, M. S. Islam and M. S. Ahsan, *Sci. Rep.*, 2023, **13**, 6050.
70 Y. Bao, S. Liu, N. Shao, Z. Tian and X. Zhu, *Colloids Surf., A*, 2023, **676**, 132266.
71 I. O. Saheed, E. N. M. Yusof, W.-D. Oh, M. A. K. M. Hanafiah and F. B. M. Suah, *Int. J. Biol. Macromol.*, 2023, **242**, 124798.
72 H. Abdolmohammad-Zadeh, Z. Ayazi and M. Veladi, *J. Iran. Chem. Soc.*, 2023, **20**, 1257–1270.
73 R. El Kaim Billah, I. Ayouch, Y. Abdellaoui, Z. Kassab, M. A. Khan, M. Agunaou, A. Soufiane, M. Otero and B.-H. Jeon, *Polymers*, 2023, **15**, 1524.
74 N. R. Azeez, S. S. Salih, M. Kadhom, H. N. Mohammed and T. K. Ghosh, *Green Chem. Eng.*, 2024, **5**, 339–347.
75 Y. Zhang, M. Haris, L. Zhang, C. Zhang, T. Wei, X. Li, Y. Niu, Y. Li, J. Guo and X. Li, *Chemosphere*, 2022, **308**, 136086.
76 K. Hachem, S. A. Jasim, M. E. Al-Gazally, Y. Riadi, G. Yasin, A. Turki Jalil, M. M. Abdulkadhm, M. M. Saleh, M. N. Fenjan and Y. F. Mustafa, *J. Chin. Chem. Soc.*, 2022, **69**, 512–521.
77 E. Guibal, *Sep. Purif. Technol.*, 2004, **38**, 43–74.